Pearl vortices in anisotropic superconducting films

V. G. Kogan[*]

Ames Laboratory–DOE, Ames, Iowa 50011, USA

N. Nakagawa

Iowa State University, Ames, Iowa 50011, USA

J. R. Kirtley

Kirtleyscientific, Pacific Grove, California 93950, USA

The magnetic field of vortices in anisotropic superconducting films is considered in the framework of an anisotropic London approach. It is found that at distances large relative to the core size, the magnetic field normal to the film surface may change sign. We find that the magnetic field attenuates at large distances as $1/r^3$ as it does in isotropic films, but the anisotropy induces an angular dependence to the supercurrents which causes the sign of the field to change for anisotropy parameters $\gamma = \lambda_2/\lambda_1 > \sqrt{2}$ in some parts of the (x, y) plane.

I. INTRODUCTION

The magnetic field distribution due to a vortex in a thin isotropic superconducting film in the (x, y) plane was evaluated by Pearl [1]. The major feature of this distribution is that the field above the film is reminiscent of one due to a magnetic "charge" ϕ_0 at the vortex core that spreads into a 2π solid angle of free space as does the electric field of the point charge. At large distances the field component h_z perpendicular to the film at the film face decays as $1/r^3$, has everywhere the same sign at the film face (positive for the vortex magnetic flux directed along $+z$), and diverges as $1/r$ if $r \ll \Lambda = 2\lambda^2/d$ (λ is the London penetration depth of the bulk material, and d is the film thickness). These features were confirmed experimentally (see, e.g., Ref. [2]).

The interest in films that are anisotropic in plane was somewhat muted mainly because of difficulties in their preparation. Films of orthorhombic materials such as YBa$_2$Cu$_3$O$_y$ (YBCO), relatively easy to grow with the c axis perpendicular to the film plane, have too small ab anisotropy to show substantial differences with isotropic films.

However, recently materials with large in-plane anisotropy were discovered. Scanning tunneling microscopy (STM) studies of films made of these materials show vortex core anisotropies of about 2.5–3.5 [3–5]. The question then arises whether vortices in films of these materials have the same Pearl form just amended with a proper rescaling. In this paper we show that this is not the case. The magnetic field structure of anisotropic Pearl vortex differs qualitatively from its isotropic version. In particular, for large enough anisotropy the field crossing the film may change sign in some patches of

the x, y plane, nevertheless keeping the total flux associated with the vortex equal to the flux quantum ϕ_0.

II. THIN FILMS

We begin with the outline of our approach for isotropic films. Let a film of thickness d be in the xy plane. Integration of the London equation for the magnetic field, $\boldsymbol{h} - \lambda^2 \nabla^2 \boldsymbol{h} = \phi_0 \hat{z} \delta(\boldsymbol{r})$, over the film thickness gives for the z component of the field at the film

$$\frac{2\pi \Lambda}{c} \text{curl}_z \boldsymbol{g} + h_z = \phi_0 \delta(\boldsymbol{r}). \tag{1}$$

Here, $\boldsymbol{g}$ is the sheet current density related to the tangential field components at the upper film face by $2\pi \boldsymbol{g}/c = \hat{z} \times \boldsymbol{h}$; $\Lambda = 2\lambda^2/d$ is the Pearl length. With the help of div $\boldsymbol{h} = 0$ this equation is transformed to

$$h_z - \Lambda \frac{\partial h_z}{\partial z} = \phi_0 \delta(\boldsymbol{r}). \tag{2}$$

A large contribution to the energy of a vortex in a thin film comes from stray fields [1]. The problem of a vortex in a thin film is, in fact, reduced to that of the field distribution in free space subject to the boundary condition supplied by solutions of Eq. (1) at the film surface. Since outside the film curl $\boldsymbol{h} = \text{div } \boldsymbol{h} = \boldsymbol{0}$, one can introduce a scalar potential for the *outside* field in the upper half space:

$$\boldsymbol{h} = \nabla \varphi, \quad \nabla^2 \varphi = 0. \tag{3}$$

The general form of the potential satisfying the Laplace equation that vanishes at $z \to \infty$ is

$$\varphi(\boldsymbol{r}, z) = \int \frac{d^2 \boldsymbol{k}}{4\pi^2} \varphi(\boldsymbol{k}) e^{i\boldsymbol{k} \cdot \boldsymbol{r} - kz}. \tag{4}$$

[*]kogan@ameslab.gov

Here, $\boldsymbol{k} = (k_x, k_y)$, $\boldsymbol{r} = (x, y)$, and $\varphi(\boldsymbol{k})$ is the two-dimensional (2D) Fourier transform of $\varphi(\boldsymbol{r}, z = 0)$. In the lower half space one has to replace $z \to -z$ in Eq. (4).

One applies now the 2D Fourier transform (FT) to Eq. (2) to obtain

$$h_{z\boldsymbol{k}} = -k\varphi_{\boldsymbol{k}} = \frac{\phi_0}{1 + \Lambda k}. \tag{5}$$

As mentioned above, the sheet current is related to the tangential field components by

$$\frac{2\pi}{c} g_x = -h_y, \qquad \frac{2\pi}{c} g_y = h_x. \tag{6}$$

In 2D Fourier space, $h_{x\boldsymbol{k}} = ik_x\varphi_{\boldsymbol{k}}$ and $h_{y\boldsymbol{k}} = ik_y\varphi_{\boldsymbol{k}}$ and we obtain

$$g_{x\boldsymbol{k}} = -g_{y\boldsymbol{k}}\frac{k_y}{k_x} = \frac{c\phi_0}{2\pi}\frac{ik_y}{k(1 + k\Lambda)}. \tag{7}$$

Thus, the field $\boldsymbol{h}$ in the free space and at the film along with the currents can be expressed in terms of the potential φ. It is easy to see that streamlines of the current coincide with contours of $\varphi(x, y) = \text{const}$. Moreover, the self-energy of a Pearl vortex and the interaction energy of two vortices can be expressed in terms of φ [6].

A. Magnetic flux of a Pearl vortex

Equation (5) gives the Fourier transform of the field h_z at the film surface. At a finite height z above the film,

$$h_z(\boldsymbol{k}, z) = \frac{\phi_0 e^{-kz}}{1 + \Lambda k} \tag{8}$$

and

$$h_z(\boldsymbol{r}, z) = \frac{\phi_0}{4\pi^2} \int \frac{d^2\boldsymbol{k}\, e^{i\boldsymbol{k}\boldsymbol{r} - kz}}{1 + \Lambda k}. \tag{9}$$

As described in Appendix A, this can be transformed to

$$h_z(R, Z) = \frac{\phi_0}{2\pi\Lambda^2} \int_0^\infty du \frac{e^{-u}(u + Z)}{[R^2 + (u + Z)^2]^{3/2}}, \tag{10}$$

where $R = r/\Lambda$ and $Z = z/\Lambda$.

Now, one can calculate the flux through a circle of the radius R:

$$\Phi_z(R, Z) = \Lambda^2 \int_0^R 2\pi R\, dR\, h_z(R, Z)$$
$$= \phi_0 \left(1 - \int_0^\infty \frac{du\, e^{-u}(u + Z)}{\sqrt{R^2 + (u + Z)^2}}\right). \tag{11}$$

For $R \to \infty$, one can replace the denominator here by R to obtain

$$\phi_0 - \Phi_z(R, Z) \sim \phi_0 \frac{1 + Z}{R}. \tag{12}$$

Hence, Φ_z approaches ϕ_0 very slowly as $1/R$. The flux $\Phi_z(R)$ is plotted in Fig. 1 for $Z = 0, 0.1, 0.5$. It is seen that even for $r = 10\Lambda$, the flux reaches only $\sim 0.8\phi_0$. Note for comparison that in the bulk the flux $\Phi_z \approx 0.9998$ at $r = 10\lambda$.
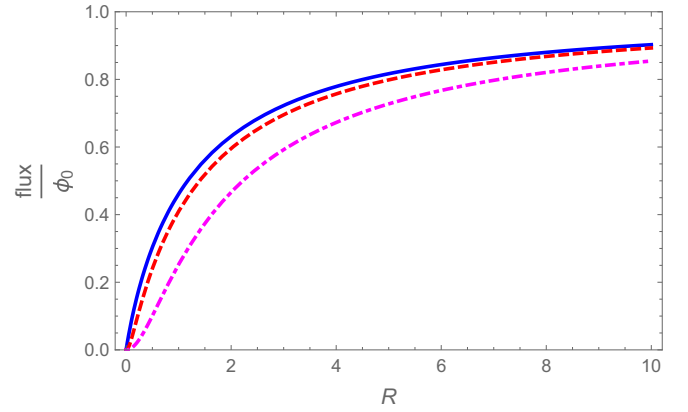

FIG. 1. The blue line is $\Phi_z(R, Z)$ for $Z = 0$, the dashed red line is for $Z = 0.1$, and the magenta dotted-dashed line is for $Z = 0.5$.

III. ANISOTROPIC FILMS

The London equations for an arbitrary oriented vortex in an anisotropic material have been given in Ref. [7]. In general, the results are cumbersome, so here we consider a simple situation of an orthorhombic superconductor in a field along the c axis. The London equation for the vortex along z in the bulk is

$$h_z + \frac{4\pi}{c}\left(\lambda_{yy}^2 \frac{\partial J_y}{\partial x} - \lambda_{xx}^2 \frac{\partial J_x}{\partial y}\right) = \phi_0\delta(\boldsymbol{r}). \tag{13}$$

Here, the frame x, y, z is chosen to coincide with a, b, c of the crystal, $\boldsymbol{r} = (x, y)$, and λ_{xx}^2 and λ_{yy}^2 are the diagonal components of the tensor $(\lambda^2)_{ik}$. A thin film of this material is assumed to be in the (x, y) plane. Integrating this over the film thickness, one obtains

$$h_z + \frac{2\pi}{c}\left(\Lambda_{yy} \frac{\partial g_y}{\partial x} - \Lambda_{xx} \frac{\partial g_x}{\partial y}\right) = \phi_0\delta(\boldsymbol{r}), \tag{14}$$

where $\boldsymbol{g} = \boldsymbol{J}d$ is the sheet current and $\Lambda_{xx} = 2\lambda_{xx}^2/d = \Lambda_1$ and $\Lambda_{yy} = 2\lambda_{yy}^2/d = \Lambda_2$ are the principal Pearl lengths. Taking into account Eq. (6) we obtain for the field components at the film surface

$$h_z + \Lambda_2 \frac{\partial h_x}{\partial x} + \Lambda_1 \frac{\partial h_y}{\partial y} = \phi_0\delta(\boldsymbol{r}). \tag{15}$$

Since $h_{x\boldsymbol{k}} = ik_x\varphi_{\boldsymbol{k}}$, $h_{y\boldsymbol{k}} = ik_y\varphi_{\boldsymbol{k}}$, and $h_{z\boldsymbol{k}} = -k\varphi_{\boldsymbol{k}}$, the 2D FT yields the potential [8,9]

$$\varphi_{\boldsymbol{k}} = -\frac{\phi_0}{k + \Lambda_1 k_y^2 + \Lambda_2 k_x^2}. \tag{16}$$

Introduce now the anisotropy parameter $\gamma^2 = \Lambda_2/\Lambda_1$ and $\Lambda = \sqrt{\Lambda_1\Lambda_2}$ so that $\Lambda_2 = \Lambda\gamma$ and $\Lambda_1 = \Lambda/\gamma$ and take Λ as the unit length,

$$h_{z\boldsymbol{q}} = -q\varphi_{\boldsymbol{q}} = \frac{\phi_0 q}{q + q_x^2\gamma + q_y^2/\gamma}, \qquad \boldsymbol{q} = \boldsymbol{k}\Lambda. \tag{17}$$
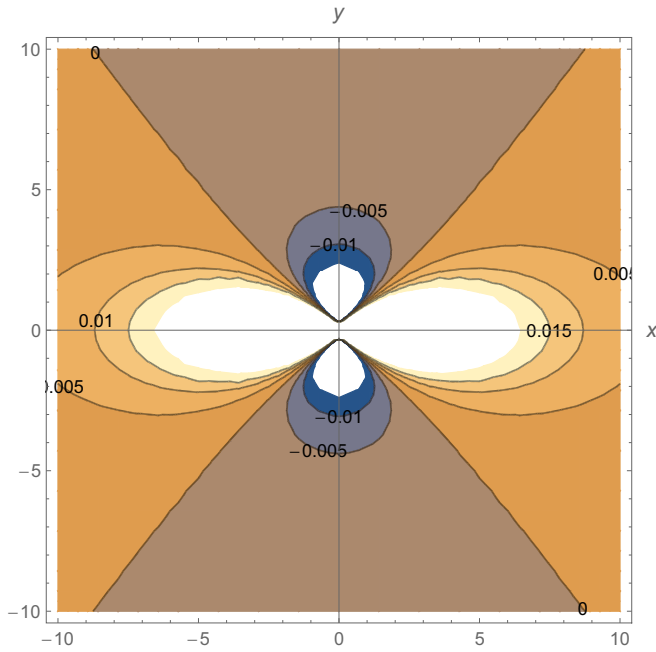
FIG. 2. Contours of $h_z(X, Y) = $ const for $Z = 0$ (h_z is in units $\phi_0/2\pi\Lambda^2$ and X, Y are in units of Λ) for $\gamma = 3$.

A. Distribution of h_z

At a finite height z above the film,

$$h_z(\boldsymbol{q}, z) = \frac{\phi_0 \, q \, e^{-qZ}}{q + q_x^2 \gamma + q_y^2/\gamma}. \quad (18)$$

Hence,

$$h_z(\boldsymbol{R}, Z) = \frac{\phi_0}{4\pi^2} \int \frac{d^2\boldsymbol{q} \, q \, e^{i\boldsymbol{q}\boldsymbol{R} - qZ}}{q + q_x^2 \gamma + q_y^2/\gamma}, \quad (19)$$

where $\boldsymbol{R} = \boldsymbol{r}/\lambda$ and $Z = z/\Lambda$.

Let us consider the field h_z at the film surface, i.e., $Z = 0$. There are two possibilities of dealing with the integral (19). The first is a "brute force" 2D fast Fourier transform (FFT). The second is to reduce—if possible—the 2D integral over $\boldsymbol{q}$ to a single integration which would be amenable for numerical evaluation. The second possibility is described in Appendix B with the result

$$h_z \frac{2\pi\Lambda^2}{\phi_0} = -\frac{1}{2} \int_0^\infty \frac{d\eta}{\sqrt{\mu\nu}} \left(\frac{1}{\rho} - \frac{\eta}{2} \right) e^{-\eta\rho/2},$$
$$\mu = 1 + \eta\gamma, \quad \nu = 1 + \eta/\gamma,$$
$$\rho = \sqrt{\frac{X^2}{\mu} + \frac{Y^2}{\nu}}. \quad (20)$$

An example of the field distribution according to this equation is given in Fig. 2. There are two major unexpected features in this result. The first is that the contours $h_z(X, Y) = $ const are not elliptic. The second and the most surprising one is that there are parts of the X, Y plane where the field is negative. Figure 3 shows that $h_z(0, Y)$ is positive in the vicinity of the singularity at $X = Y = 0$, turns zero at $Y \approx 0.3$, changes sign, and, after reaching a negative minimum near $Y \approx 0.5$, decays to -0 as $Y \to \infty$. It is worth noting that in an infinite
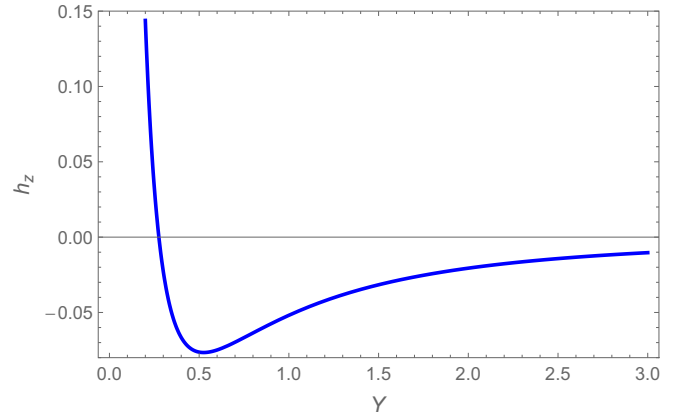

FIG. 3. $h_z(0, Y)$ (h_z is in units $\phi_0/2\pi\Lambda^2$ and X, Y are in units of Λ) for $\gamma = 3$.

isotropic film the field h_z crossing the film has the same sign everywhere, i.e., after crossing the film the stray field lines go to infinity, never crossing the film again. Although the possibility of the field h_z changing sign in anisotropic films was noted some time ago [8], the phenomenon was not studied in any detail.

One can derive analytically the asymptotic behavior of the field as $R \to \infty$. Omitting details we present the result

$$h_z \frac{2\pi\Lambda^2}{\phi_0} = \frac{1}{2R^3\gamma} \left[\gamma^2 + 1 + 3(\gamma^2 - 1)\frac{X^2 - Y^2}{R^2} + O(R^{-1}) \right]. \quad (21)$$

The second term here does not survive in the isotropic case, whereas for anisotropic films it describes the angular-dependent part, $(X^2 - Y^2)/R^2 = \cos 2\alpha$, where α is the azimuth counted from the X axis. At large distances the lines where $h_z(X, Y) = 0$ are given by

$$\cos 2\alpha = -\frac{\gamma^2 + 1}{3(\gamma^2 - 1)}. \quad (22)$$

Hence, we obtain a restriction on γ for this solution to exist, $\gamma > \sqrt{2}$. For $\gamma \gg 1$, $\cos 2\alpha = -1/3$, i.e., $\alpha = 54.7°$, and the opening angle of the domain of negative h_z is $\sim 70.6°$.

Since the profile $h_z(X, Y)$ shown in Fig. 2 is highly unusual and was obtained after an involved analytical procedure, to be confident we applied the 2D FFT directly to the double integral of Eq. (19). The result shown in Fig. 4 confirms the existence of the negative domain. Moreover, it allows one to estimate the negative fraction of the flux as $\sim 10\%$ of the flux quantum ϕ_0 for $\gamma = 3$ at $Z = 0$.

The behavior of $h_z(X, Y)$ at shorter distances $-1 < (X, Y) < 1$ is shown in Fig. 5. Note that these distances $\sim\Lambda$ are still large relative to the core size, so that we are still in the region where the London approach holds.

B. Z dependence

All methods of studying Pearl vortices use sensors placed at a certain height above the film and measuring $h_z(\boldsymbol{r}, z)$ at a
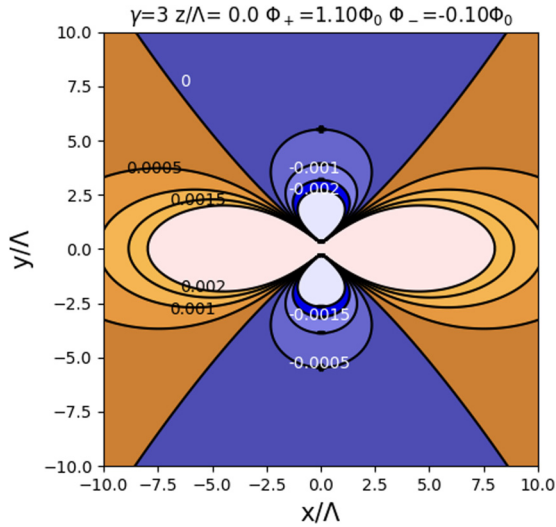
FIG. 4. $h_z(X, Y)$ (in units ϕ_0/Λ^2 and X, Y in units of Λ) for $\gamma = 3$ in the window $-10 < X, Y < 10$ obtained by using 2000×2000 pixel FFT in a cell $-50 < X, Y < 50$. Here, the pink regions (horizontal lobes) have $h_z > 0.002$ and the light blue regions (vertical lobes) have $h_z < -0.002$. Φ_+ is the integrated flux of positive $h_z(X, Y)$ over the entire $50\Lambda \times 50\Lambda$ area and Φ_- is the integrated flux of negative $h_z(X, Y)$ over the same area

small but finite z. Hence, it is of interest to see what Eq. (19) generates in the case of anisotropic films. The series of $h_z(r, z)$ profiles obtained with the help of FFT is shown in Figs. 6–8. The negative flux, which is $\approx 0.10\phi_0$ for $Z = 0$, decreases to $0.06\phi_0$ for $Z = 0.1$, to $0.04\phi_0$ for $Z = 0.2$, and to $0.01\phi_0$ for $Z = 0.5$.
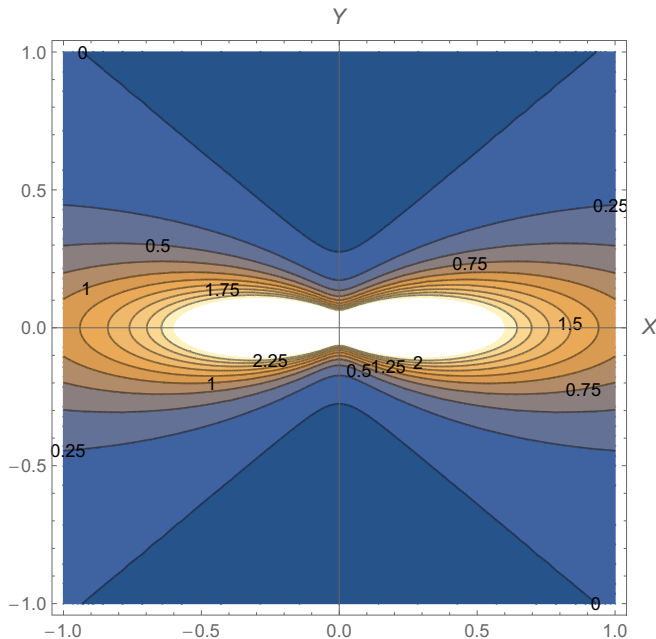

FIG. 5. $h_z(X, Y)$ for $\gamma = 3$ for a shorter distances $-1 < (X, Y) < 1$. The darkest part is the region of negative h_z.
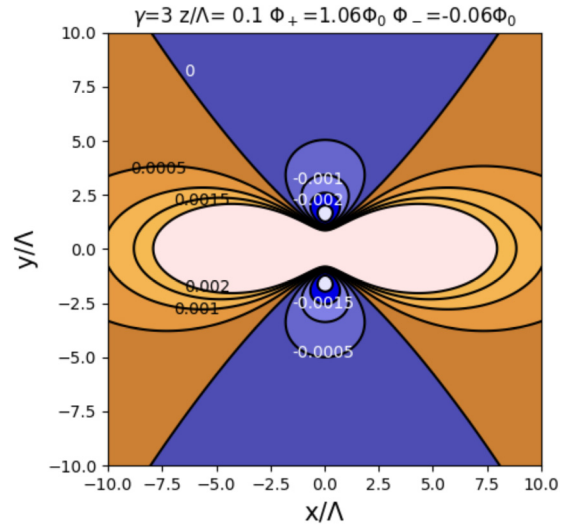

FIG. 6. FFT evaluation of $h_z(X, Y)$ in units ϕ_0/Λ^2 for $Z = 0.1$ done for $-50 < (X, Y) < 50$, but the result is shown in the window $-10 < (X, Y) < 10$.

In fact, it is possible to get the $h_z(R, Z)$ analytically as a 1D integral in the same manner as Eq. (20) was derived,

$$h_z \frac{2\pi \Lambda^2}{\phi_0} = \frac{1}{2} \int_0^\infty \frac{d\eta}{\sqrt{\mu\nu}} \left[\frac{\eta}{2} - \frac{1 - \eta Z}{\rho} \right.$$
$$\left. + \frac{Z^2(\eta\rho + 2)}{2\rho^3} \right] \exp\left[-\frac{\eta(\rho + Z)}{2} \right],$$
$$\rho = \sqrt{\frac{X^2}{\mu} + \frac{Y^2}{\nu} + Z^2}. \tag{23}$$

where μ, ν are given in Eq. (20).

One can also estimate the negative fraction of the flux $\Phi_z = \int d^2 r h_z(r)$. To this end, we did this with the help of both FFT and employing $h_z(R, Z)$ of Eq. (23). One should

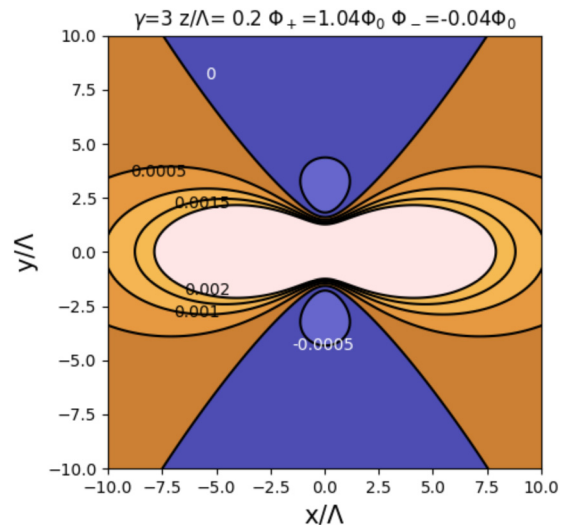FIG. 7. FFT evaluation of $h_z(X, Y)$ in units ϕ_0/Λ^2 for $Z = 0.2$ done for $-50 < (X, Y) < 50$, but the result is shown in the window $-10 < (X, Y) < 10$ for $Z = 0.2$.
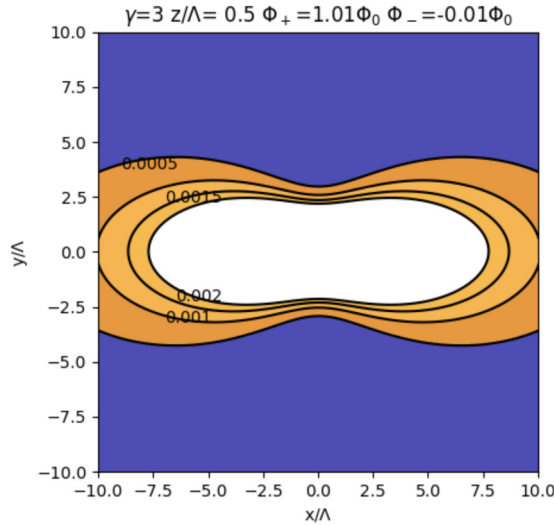
FIG. 8. FFT evaluation of $h_z(X, Y)$ in units ϕ_0/Λ^2 done for $-50 < (X, Y) < 50$, but the result is shown in the window $-10 < (X, Y) < 10$ for $Z = 0.5$.

be careful applying FFT to the problem of a single vortex, since within FFT one has to choose a large patch of the XY plane as a unit cell of the periodic lattice covering the whole plane to apply periodic boundary conditions. The hope then is that for a large enough unit cell, say, $(50 \times 50)\Lambda$, the field of the vortex is small enough near the cell boundaries where the field distortions by periodic boundary conditions do not matter. Doing this one has to require the flux Φ_z through the cell $(50 \times 50)\Lambda$ be ϕ_0. This procedure works well in the bulk where the vortex field decays exponentially, and choosing an FFT cell of a few λ one gets Φ_z very close to ϕ_0. In thin films, however, $(\phi_0 - \Phi_z)$ decreases extremely slow as $1/r$ with r being the cell linear size. Hence, to have accurate FFT output one has to choose a large FFT unit cell, e.g., $(50 \times 50)\Lambda$, and consider only a central part of the cell, say, $(10 \times 10)\Lambda$, where the effects of boundaries are weak and the results are reliable. That is how Figs. 4 and 6–8 were obtained. Repeating the FFT analysis over a larger $(100 \times 100)\Lambda$ area results in positive and negative fluxes $\sim 1\%$ different than reported here for a $(50 \times 50)\Lambda$ area.

Now, the 1D integral representation of $h_z(\boldsymbol{R}, Z)$, Eq. (23), is equivalent to the original 2D integral over q_x, q_y, Eq. (19)—in other words, it is a solution of the vortex problem on the infinite x, y plane which satisfies the condition $\Phi_z = \phi_0$. Unlike FFT, we start here with the exact solution, choosing, say, the $(10 \times 10)\Lambda$ window, and calculate the negative flux in this window.

We conclude this section with the plot of $h_z(0, Y)$ along the Y axis in Fig. 9 and of the integrated negative flux at a set of heights Z.

C. Potential and currents

Manipulations, similar to those used for deriving $h_z(\boldsymbol{r})$, using Eq. (19) for the potential $\varphi(\boldsymbol{q})$, give in real space

$$\varphi(\boldsymbol{r}) = -\frac{\phi_0}{4\pi} \int_0^\infty \frac{d\eta}{\sqrt{\mu\nu}} e^{-\eta\rho/2}, \qquad (24)$$
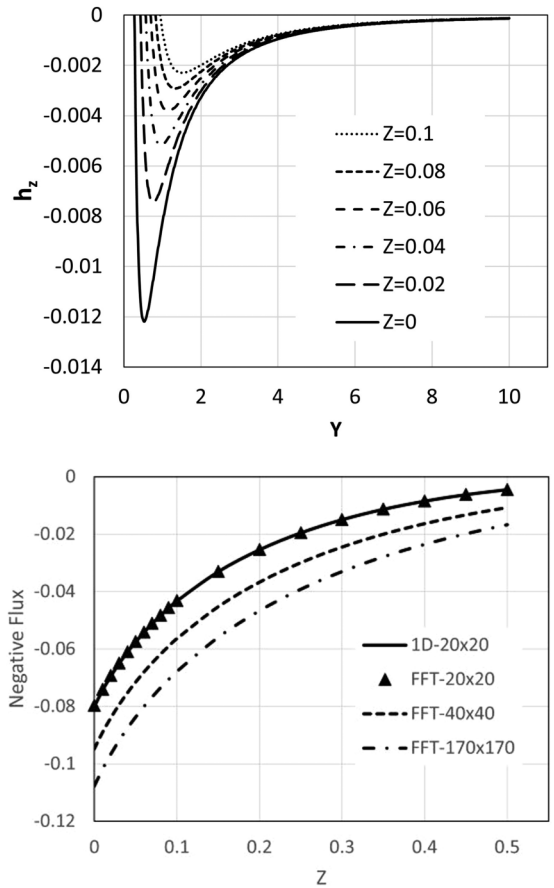

FIG. 9. The upper panel: $h_z(0, Y)$ in units $\phi_0/2\pi\Lambda^2$ for $Z = z/\Lambda$ indicated in the legend. The lower panel: The negative flux in units ϕ_0 vs the lift Z. All FFT lines were obtained using results from FFT on a very large unit cell 170×170. These "data" were then scanned through smaller windows indicated in the legend. The upper solid curve is obtained by evaluating numerically the 1D integral of Eq. (23) for the field distribution and then by integration (summation) over the window area 20×20. The 1D integral is computed pointwise in 0.01 steps. Note the good agreement with the FFT results in this window shown by solid triangles.

where μ, ν, and ρ are defined in Eq. (20).

At large distances $r \gg \Lambda$ only small q are relevant, so that the term $q_y^2/\gamma + q_x^2\gamma$ can be discarded in Eq. (17) that implies that the potential there is isotropic. Physically the field there should correspond to that of a point "magnetic charge" ϕ_0 in the solid angle 2π (in the upper half space), i.e., $\varphi(r) = -\phi_0/2\pi r$. This conclusion could also be reached using Eq. (24): For $\rho \to \infty$ the relevant $\eta \to 0$ is due to the exponential factor. Hence, $\mu \sim \nu \sim 1$ and the remaining integral gives $\varphi(r) = -\phi_0/2\pi r$.

The streamlines of current are given by $(\boldsymbol{g} \times d\boldsymbol{L})_z = g_x dy - g_y dx = 0$, and $d\boldsymbol{L} = (dx, dy)$ is the line element. This translates to $\varphi = \text{const}$, whose contours are shown in Figs. 10 and 11, where these contours are in fact the current lines. One sees that the current anisotropy decreases with increasing distance, but—at first sight—noting in current distributions that might suggest an unusual behavior of $h_z(X, Y)$.

As shown in Ref. [6], the interaction energy of a vortex at the origin with another one at (x, y) is $\phi_0\varphi(\boldsymbol{r})/4\pi$. In fields
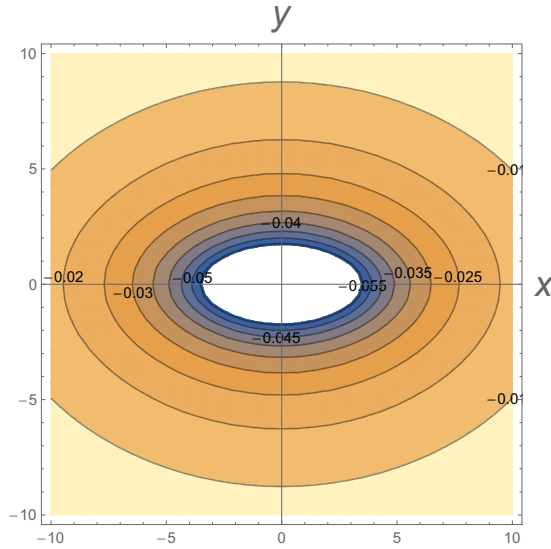
FIG. 10. Contours of $\varphi(X, Y) = $ const. X, Y are in units of Λ for $\gamma = 3$.

H applied perpendicular to the film, the distance between vortices in the flux-line lattice is $\propto \sqrt{\phi_0/H}$. Therefore, with increasing applied field H, the anisotropy of contours $\varphi = $ const increases along with the anisotropy parameter of the vortex lattice. The commonly used assumption that the lattice anisotropy is field independent and fixed by the anisotropy of the penetration depth should be used with care. The same can be said about extracting the anisotropy parameter of the film material from the geometry of the flux-line lattice.

IV. DISCUSSION

In thin films there is no usual differential relation between the in-plane current and the field h_z, so the Maxwell equation curl $\boldsymbol{h} = 4\pi \boldsymbol{j}/c$ is replaced by boundary conditions at the film
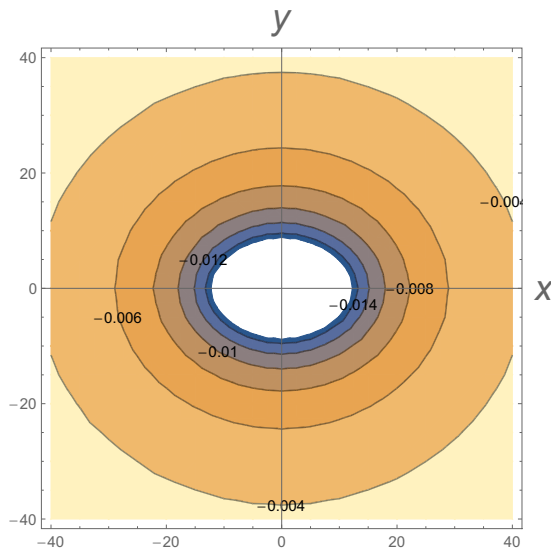

FIG. 11. Contours of $\varphi(X, Y) = $ const at larger distances. X, Y are in units of Λ for $\gamma = 3$.

which relate the sheet current $\boldsymbol{g}$ to tangential fields. The common way to evaluate the h_z is to use the Biot-Savart integral relation between h_z and $\boldsymbol{g}$. In our approach, both fields and currents are expressed in terms of the potential φ.

London equations *per se* are conditions of minimum of the London energy (magnetic+kinetic) [10]. The $h_z(x, y)$ solutions of these equations, however strange they may look, correspond to the minimum energy. Therefore, the fact that the vortex magnetic field lines in anisotropic films may prefer to cross the film from the upper half space to the lower one in some parts of the xy plane, unlike the case of isotropic films where these lines go to infinity without crossing the film again, should be seen as a way the vortex system minimizes its energy. It is worth noting that this situation emerges when the current anisotropy decreases with the distance from the vortex core as shown in Figs. 10 and 11.

It is instructive to consider an example of the field h_z at the film created by two concentric current loops in the xy plane, the small one strongly elongated in the x direction with a large current and the big circular loop with a small current. Both currents are in the same, say, counterclockwise direction so that their contributions to h_z inside a small loop are both positive. However, outside the smaller loop in its vicinity the contribution of the large current of this loop is negative and cannot be canceled by a positive contribution of the distant loop. This cancellation cannot happen also because the large loop is a circle whereas the small one is elliptic. One can also give a qualitative argument why the domain of the negative field is situated near the y axis.

Hence, although the "strange" field distribution of Figs. 2–5 is a consequence of Maxwell and London equations and as such do not bring in any new physics, our result is relevant for the interpretation of data when the normal field component above the film surface is measured such as by the scanning superconducting quantum interference device (SQUID) or magnetic force microscopies. These techniques are currently fast improving (see, e.g., Ref. [11]), and confirming the sign change of the normal field component may become feasible.

Most of our calculations were done for orthorhombic materials with an in-plane anisotropy parameter $\gamma = 3$ and the vortex along c. Such materials in fact exist, with examples being NiBi films [3] or $Ta_4Pd_3Te_{16}$ [4].

APPENDIX A: $H_z(R, Z)$ IN ISOTROPIC FILMS

Rewrite Eq. (9) using Λ as a unit length and $\phi_0/2\pi\Lambda^2$ as a unit of field,

$$H_z(\boldsymbol{R}, Z) = h_z(\boldsymbol{r}, z)\frac{2\pi\Lambda^2}{\phi_0} = \frac{1}{2\pi}\int \frac{d^2q\, e^{i\boldsymbol{q}\boldsymbol{R}-qZ}}{1+q}, \quad \text{(A1)}$$

where the dimensionless $q = k\,\Lambda$, $R = r\,\Lambda$, and $Z = z/\Lambda$. With the help of the identity

$$\frac{1}{1+q} = \int_0^\infty e^{-u(1+q)}du, \tag{A2}$$

one rewrites the field as

$$H_z(\boldsymbol{R}, Z) = \frac{1}{2\pi} \int_0^\infty du\, e^{-u} \int d^2\boldsymbol{q}\, e^{i\boldsymbol{q}\cdot\boldsymbol{R} - q(u+Z)}. \tag{A3}$$

To evaluate the last integral over $\boldsymbol{q}$, we note that the three-dimensional (3D) Coulomb potential is

$$\frac{1}{4\pi\mathcal{R}} = \frac{1}{(2\pi)^3} \int \frac{d^3\boldsymbol{Q}}{Q^2}\, e^{i\boldsymbol{Q}\cdot\mathcal{R}}, \tag{A4}$$

where $\boldsymbol{Q} = (\boldsymbol{q}, Q_z)$, $\mathcal{R} = (\boldsymbol{R}, Z)$, and $d^3\boldsymbol{Q} = d^2\boldsymbol{q}\, dq_z$. Integration over q_z is doable,

$$\int_{-\infty}^\infty \frac{dq_z}{2\pi} \frac{e^{iq_z Z}}{q^2 + q_z^2} = \frac{e^{-q|Z|}}{2q}, \tag{A5}$$

and we obtain instead of Eq. (A4)

$$\frac{1}{\sqrt{R^2 + Z^2}} = \frac{1}{2\pi} \int \frac{d^2\boldsymbol{q}}{q}\, e^{i\boldsymbol{q}\cdot\boldsymbol{R} - qZ}. \tag{A6}$$

Applying ∂_Z to both sides, we obtain

$$\int d^2\boldsymbol{q}\, e^{i\boldsymbol{q}\cdot\boldsymbol{R} - qZ} = \frac{2\pi Z}{(R^2 + Z^2)^{3/2}}. \tag{A7}$$

To get the integral in Eq. (A3), replace $Z \to Z + u$:

$$H_z(\boldsymbol{R}, Z) = \int_0^\infty du \frac{(Z+u)\,e^{-u}}{[R^2 + (Z+u)^2]^{3/2}}. \tag{A8}$$

APPENDIX B: $H_z(\boldsymbol{R}, Z)$ IN ANISOTROPIC FILMS

Rewrite Eq. (19), using Λ as a unit length and $\phi_0/2\pi\Lambda^2$ as a unit of field. Then, transform the denominator employing Eq. (A2),

$$\begin{aligned}
H_z(\boldsymbol{R}, Z) &= h_z(\boldsymbol{r}, z)\frac{2\pi\Lambda^2}{\phi_0} = \frac{1}{2\pi} \int \frac{d^2\boldsymbol{q}\, q\, e^{i\boldsymbol{q}\boldsymbol{R} - qZ}}{q + \gamma q_x^2 + q_y^2/\gamma} \\
&= 2\pi \int_0^\infty du \int \frac{d^2\boldsymbol{q}\, q}{(2\pi)^2} e^{i\boldsymbol{q}\boldsymbol{R} - q(u+Z) - u(\gamma q_x^2 + q_y^2/\gamma)}.
\end{aligned} \tag{B1}$$

Now we use the identity Eq. (A5) in the form

$$\int_0^\infty d\xi \int_{-\infty}^\infty \frac{dq_z}{2\pi} e^{iq_z Z - \xi(q^2 + q_z^2)} = \frac{e^{-q|Z|}}{2q}. \tag{B2}$$

Applying ∂_Z twice and replacing $|Z| \to u + Z$, we obtain

$$q\, e^{-q(u+Z)} = -2 \int_0^\infty d\xi \int_{-\infty}^\infty \frac{dq_z}{2\pi} q_z^2\, e^{iq_z(u+Z) - \xi(q^2 + q_z^2)}. \tag{B3}$$

Hence, we have

$$\begin{aligned}
H_z(\boldsymbol{R}, Z) &= -4\pi \int_0^\infty d\xi \int_0^\infty du \int \frac{d^3\boldsymbol{Q}}{(2\pi)^3} q_z^2 \exp\left[i\boldsymbol{q}\boldsymbol{R} + iq_z(u+Z) - u(\gamma q_x^2 + q_y^2/\gamma) - \xi(q^2 + q_z^2) \right], \\
\boldsymbol{Q} &= (\boldsymbol{q}, q_z).
\end{aligned} \tag{B4}$$

The required expressions, Eqs. (20) and (23), can be obtained in the following tedious but straightforward procedure: (1) Change the variables as $\xi \to \eta$ according to $\xi = u/\eta$, (2) perform the Gaussian integrations over $\boldsymbol{Q}$, and then (3) integrate over u, leaving the remaining η integration to be performed numerically. In particular, the u integration can be performed analytically according to the

formula

$$\int_0^\infty du\, u^{\nu-1} \exp(-\alpha^2 u - \beta^2/u) = 2(\beta/\alpha)^\nu K_\nu(2\alpha\beta), \tag{B5}$$

where $K_\nu(z)$ is the modified Bessel function of the second kind [12], e.g.,

$$K_{1/2}(z) = \sqrt{\pi/2z}\,e^{-z}, \quad K_{3/2}(z) = \sqrt{\pi/2z}\,(1 + z^{-1})e^{-z}. \tag{B6}$$

[1] J. Pearl, Appl. Phys. Lett **5**, 65 (1964).

[2] F. Tafuri, J. R. Kirtley, P. G. Medaglia, P. Orgiani, and G. Balestrino, Phys. Rev. Lett. **92**, 157006 (2004).

[3] W.-L. Wang, Y.-M. Zhang, Y.-F. Lv, H. Ding, L. Wang, W. Li, K. He, C.-L. Song, X.-C. Ma, and Q.-K. Xue, Phys. Rev. B **97**, 134524 (2018).

[4] Y. Fujimori, S. I. Kan, B. Shinozaki, and T. Kawaguti, J. Phys. Soc. Jpn. **69**, 3017 (2000).

[5] Z. Du, D. Fang, Z. Wang, Y. Li, G. Du, H. Yang, X. Zhu, and H.-H. Wen, Sci. Rep. **5**, 9408 (2015).

[6] V. G. Kogan, Phys. Rev. B **75**, 064514 (2007).

[7] V. G. Kogan, Phys. Rev. B **24**, 1572 (1981).

[8] V. G. Kogan, A. Yu. Simonov, and M. Ledvij, Phys. Rev. B **48**, 392 (1993).

[9] V. G. Kogan and R. Prozorov, Phys. Rev. B **102**, 184514 (2020).

[10] P. de Gennes, *Superconductivity of Metals and Alloys* (Benjamin, New York, 1966).

[11] L. Embon, Y. Anahory, Ž. L. Jelić, E. O. Lachman, Y. Myasoedov, M. E. Huber, G. P. Mikitik, A. V. Silhanek, M. V. Milosević, A. Gurevich, and E. Zeldov, Nat. Commun. **8**, 85 (2017).

[12] *Handbook of Mathematical Functions*, edited by M. Abramowitz and A. Stegun (U.S. Government Printing Office, Washington, D.C., 1972).